JOURNAL OF NANO- AND ELECTRONIC PHYSICS
Vol. **5** No 1, 01016(8pp) (2013)

ЖУРНАЛ НАНО- ТА ЕЛЕКТРОННОЇ ФІЗИКИ
Том **5** № 1, 01016(8cc) (2013)

High Dose Ion Implantation Into NiTi for Improvement of Pseudoplasticity and Shape Memory Effect

A. Pogrebnjak[1,*], S. Bratushka[1], N. Levintant-Zayonts[2]

[1] *Sumy State University, 2, Rimsky-Korsakov Str., Sumy, 40007 Ukraine*
[2] *Institute of Fundamental Technological Research, PAS, 21 Swietokrzyska str, 00-049 Warsaw*

(Received 24 October 2012; published online 28 March 2013)

New investigation results of N^+, Mo, W, N and Ni high dose ion implantation of $10^{18}cm^{-2}$ influence on alloys physical and mechanical properties are presented in this article. Increasing of alloys wear resistance by abrasion of the surface layer, increasing of nanohardness, corrosion resistance, and changes of surface NiTi morphology are obtained. The correlation between the change of the elemental composition (after implantation) and the increase in mechanical properties of the alloy is observed. In other words, a nanostructure of oxycarbides and oxynitrides is formed in the surface layer as a result of high-dose ion implantation, which improves wear resistance, corrosion resistance and nanohardness of material. At the same time, the bulk properties of NiTi after implantation (pseudoplasticity and shape memory effect) do not change, which makes ion implantation an effective tool for improvement materials properties.

Keywords: Implantation, NiTi, Shape memory effect, Pseudoelastic, Properties.

PACS numbers: 61.72.up, 62.20.Qp, 68.35.bd

1. INTRODUCTION

Shape memory alloys (SMAs) possess an array of desirable properties: high power to weight ratio, thus the ability to recover large transformation stress and strain upon heating and cooling, pseudoelasticity (PE), high damping capacity, good chemical resistance and biocompatibility. This attracted much attention to the research of SMAs as smart and functional materials [1]. Among these SMA films, NiTi based films are the most promising.

Research related to application of NiTi alloys in medicine started in the late sixties. NiTi alloys became attractive for medical applications particularly because of memory properties. Ability of NiTi elements to recover an original shape after being deformed up to almost 10 % offers a considerable improvement during numerous medical treatments. For instance, a tailored compressive fixation of bone fragments (e.g. fragments of small bones, broken jaws, cranial fractures) can be easily performed using recoverable deformation. Anchoring of implants (e.g. tooth roots, joint implants) and dentures to the living tissues as well as positioning of tissues (e.g.. shifting of misaligned teeth or vertebra, opening of narrowed veins or urethral tracts) is easily achievable using NiTi articles exhibiting shape memory behavior. Forces generated by memory elements can be controlled and invasive interventions can be minimized. Actuating ability of shape memory articles allows replacement or support of damaged muscles and tendons. Unique memory properties allow to design unique medical instruments with excellent steerability and flexibility (e.g. endoscopes). In addition to memory properties, NiTi shape memory alloys exhibit significantly better mechanical compatibility with tissues compared to other alloys and ceramics used in medicine. NiTi alloys exhibit excellent corrosion resistance, wear resistance, mechanical damping capacity, MRI visibility and sufficient radio-opacity [2].

The phase transformation in SMA thin film is accompanied by significant changes in the mechanical, physical, chemical, electrical and optical properties, such as yield stress, elastic modulus, hardness, damping, shape recovery, electrical resistivity, thermal conductivity, thermal expansion coefficient, surface roughness, vapor permeability, dielectric constant, etc. These changes can be fully made using the design and fabrication of microsensors and microactuators. The fatigue life and sharpness of the NiTi tool is excellent compared to steel because of SIM formation and greater wear resistance and corrosion stability. The PE and SME were also utilized in instruments with a non-traumatic tissue retractor, repositioning devices [3] or markers. Chisels, scissor forceps, saws and blades made of NiTi alloys, which do not use SME or PE are effective due to their excellent wear and corrosion resistance. However, due to the lack of full understanding of the thin film SMAs together with the difficulty in controlling of the deposition parameters, they have not received as much attention in the technology as other microactuator technologies [2].

The introduction of a third component (Si or B) into the films may markedly improve their physico-mechanical properties and thus extend the scope of application. Chromium is known to have a beneficial effect on the stability of titanium carbides, borides and nitrides against oxidation and on the wear resistance of articles made of them at elevated temperatures.

The application of high-dose intense implantation leads to an increase in the ion penetration depth; intensified scattering of the surface layer; a shift in the maximum, concentration, and shape of the concentration profile; and many other processes that are weakly pronounced during low-intensity ion implantation at low doses (several units of atomic processes) of implanted ions [4-6]. On the other hand, NiTi-based alloys

* alexp@i.ua

belong to the group of materials in which a high-temperature phase with a B_2 structure undergoes a shear or martensitic phase transformation as the temperature change or a stress is applied. The atomic restructuring in NiTi-based alloys is accompanied by both martensitic anelasticity effects and a change in their surface state, which are caused by the complex structure of the martensite phase in them [7, 8].

As a result, a developed martensitic relief with a large number of various interfaces appears, which should affect both the electrochemical and corrosion properties and the plasticity and strength properties of these materials. As a method of surface alloying, ion implantation of a surface can strongly affect the structural parameters and stability of the B_2 phase in the near-surface layers and, hence, the following set of its properties: the martensite transformation temperature, the martensite anelasticity parameters, the shape memory effect (SME), and superplaslicity. As a result, it can change the deformation relief, the cracking conditions, and the electro-chemical and corrosion properties [9-14]. Therefore, double implantation of N^+ and Ni^+ ions into NiTi is of particular interest, since the implantation of Ni^+ ions changes the equiatomic composition of the alloy and. in combination with N^+ ions, hardens the surface layer and, correspondingly, modifies the physico-mechanical and chemical properties [15]. The alloying of steels and alloys with elements such as W and Mo are widely used to improve their mechanical properties; therefore, it is interesting to perform implantation of Mo^+ and W^+ ions at high doses. The purpose of this work is to study the depth profile of the elemental composition of the implanted layer, the structure and morphology of the NiTi alloy surface, and the mechanical properties of the alloy implanted by high doses of N^+, $Ni^+ + N^+$ and $W^+ + Mo^+$ ions at doses ranging from 5×10^{17} to 10^{18} cm^{-2} [16, 17].

2. METHODS OF ANALYSIS AND COATING APPLICATION

We analyzed equiatomic NiTi (51.5 % Ni) alloy samples $22 \times 5.4 \times 0.25$ mm in size. In the initial state, the samples were vacuum annealed at 803 K for 30 min followed by slow cooling. After cooling, the sample surfaces were etched with a mixture of 10 % $HClO_4$ and 90 % acetic acid. The N^+ ion implantation of the NiTi samples was performed on a semi-industrial IMJON (Warsaw) implanter at doses of 1×10^{17}, 5×10^{17}, and 10^{18} cm^{-2} at a current density of 0.8-1 mA. The implantation of Ni^+ and $Mo^+ + W^+$ ions was carried out using a vacuum-arc Diana source at a voltage of about 60 kV, a dose of 5×10^{17} cm^{-2}, and a substrate temperature of less than 250 C. Irradiation was performed at a pressure of ~ 10^{-3} Pa. The pulse duration was 200 μs, the pulse repetition frequency was 50 Hz, and the nitrogen concentration in NiTi was determined from the "eating away" in its energy spectrum. The phase-transformation temperatures were determined with a Pyris-1 differential scanning calorimeter, and the elemental composition of the samples was determined by the following methods: Auger electron spectroscopy on a PHI-660 (Perkin-Elmer) device, scanning electron microscopy on a Selmi (Sumy, Ukraine) microscope equipped with EDS and WDS microanalyses and on a Perkin-Elmer microscope, and Rutherford backscattering of ions (2.012-MeV proton beams. 2.035-MeV $^+$He ion beams). Rutherford backscattering spectra were analyzed using the standard RUMP and DWBS software packages [18] to construct the depth profiles of elements (Ni^+, Mo^+, W^+ ions). Ions backscattered at the angle of 170° were detected using a surface barrier detector with an energy resolution of 20 keV. In addition, we used a Neophot-2 optical microscope. To measure the mechanical properties and SME, we used a diamond pyramid (Brinel) microindenter) with a side of 40 nm at a load of 4, 7, 10, 13, 16 and 20 N and a Talysurt-5-120 scanning profilometer. The measurements were performed in the initial state and after ion implantation.

The microhardness on the surface of a sample and across was measured with a PMT-3 device at various loads. The nanohardness was measured with a trihedral Berkovich pyramid on a Nano Indenter II (MTS System Corp., Ridge, Tennessee, United States) nanohardness tester. To find the hardness and the elastic modulus at the maximum load, we used the Oliver-Pharr technique [19].

X-ray diffractometry, using the Philips diffractometer type X'Pert in the Bragg-Brentano geometry, was used to identify the phase composition of NiTi alloy samples in both non-implanted conditions and after implantation with nitrogen. CuK_α radiation (wavelength λ – 0.154184 nm) diffracted by the sample was selected by a graphite monochromator. The parameters of X-ray diffractometry: scanning voltage of the X-ray tube - 40 kV, the current - 25 mA, the exposure time - 10 s and the measured angle, 2Θ, - from 25° to 95°. The scanning step was 0.02°. The low temperature X-ray diffraction studies were carried out using the TTK Low-Temperature Camera (Anton Paar). The sample was heated from -50 °C up to + 150 °C in argon atmosphere. The measured angle, 2Θ,was from 35° to 47° with the scanning step of 0.02°. Lattice parameters were determined by using the Philips X'Pert Plus software for all detected peaks.

Specimens for TEM and HREM (Tecnai G^2, FEI Company) examinations were prepared by Focused Ion Beam System (FEI QUANTA 3D).

3. RESULTS AND DISCUSSION

The studies were started with DSC measurements. The sample weight of approximately 5 mg was analyzed with an empty aluminum pan as the reference. A temperature range from – 50 °C to + 150 °C was scanned at a rate of 20 °C/min during cooling and heating. Fig. 1 shows the evolution of DSC cooling/heating curves for the virgin and ion-implanted alloys. As it can be seen, the NiTi alloy transforms in two steps showing two peaks on the DSC curve in the cooling direction. The first DSC peak correlates with the transformation from the austenite (*A*) with a cubic structure (B_2-phase) to the R-phase with a rhombohedral one (referred to as a rhombohedral distortion of the austenite). The second DSC peak correlates with the transformation from the R-phase to the martensite (*M*) with a monoclinic structure ($B_{19'}$-phase).

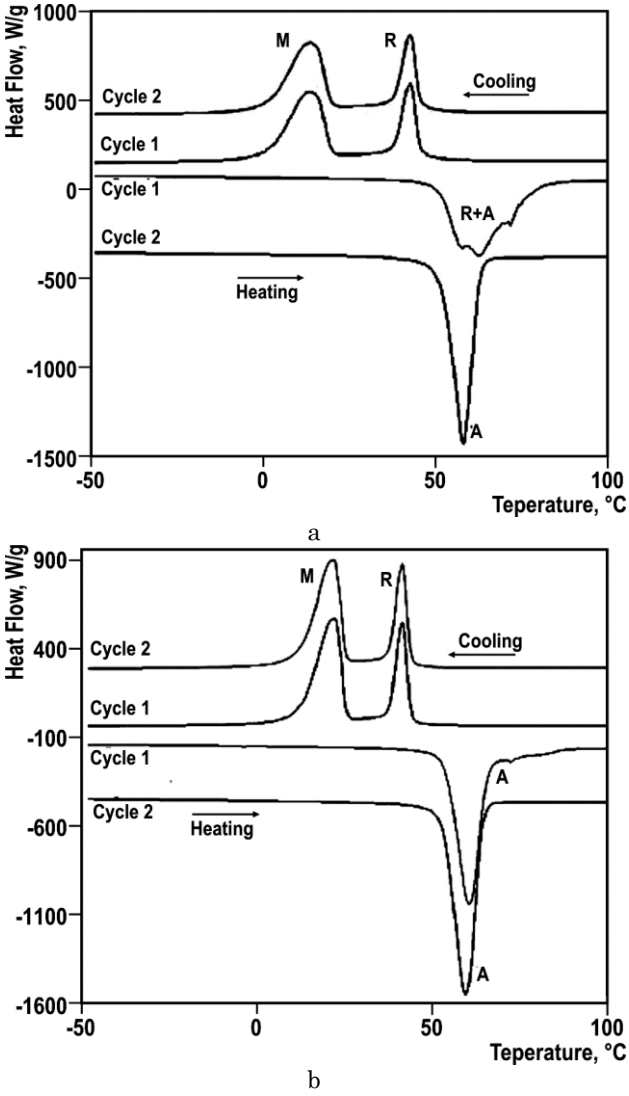

Fig. 1 – DSC curves of the virgin NiTi alloy (a) and DSC curves of ion-implanted alloys indicating a two-step phase transformation occurred during cooling (b)

Similar two-step martensite phase transition from high temperature was observed for the NiTi alloys after the thermo-mechanical treatment or solution treatment and subsequent aging. The one-step but composed transition took place during the heating process. The endothermic peak during the heating process resulted in the transition of the martensite to the austenite phase. The peak in the heating direction corresponds to the austenite (B_2-phase) with t_{start} = 51.6 °C, t_{finish} = 62.3 °C for the virgin alloy and with t_{start} = 52.5 °C, t_{finish} = 64 °C for the ion-implanted one. The subscript 'start' denotes the onset temperature at which the phase transformation starts, and the subscript 'finish' denotes the temperature at which the phase transformation finishes.

Transformation temperatures M_f, M_s, A_s, A_f, T_R as well as their changes with applied stress must be determined experimentally. Temperature dependence of yield stress has to be measured. Temperature is estimated from cross-section of M_s and $R_{P0.2}$ dependencies. Proper design requires knowledge of the deformation behavior of particular NiTi SMA element at application temperatures [2]. Dependencies shown in Fig. 2 illustrate the change in the temperature of martensitic initiation transformation.

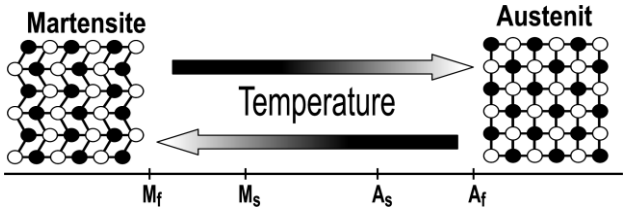

Fig. 2 – The scheme of the direction of change of the initial temperatures of the phase transitions

The two peaks in the cooling direction corresponding to the R-phase and the martensite $B_{19'}$-phase were determined to have transformation temperatures, respectively: t_{start} = 45.1 °C, t_{finish} = 37.8 °C, t_{start} = 19 °C, t_{finish} = 1 °C for the virgin alloy and t_{start} = 43.3 °C, t_{finish} = 37.4 °C, t_{start} = 24.6 °C, t_{finish} = 11.6 °C for an ion-implanted alloy. With Auger electron spectroscopy, we also studied the NiTi samples before and after implantation with nitrogen ions. In the initial state, carbon and oxygen are present near the surface; after sputtering for 15-18 min only nickel and titanium are present in the NiTi sample, and their concentrations are close to the equiatomic composition. After implantation, the nickel concentration in the surface layer decreases to almost 10 at. % because of sputtering of the surface. Since it is difficult to separate the peaks of nitrogen and titanium ions, we constructed a TiN profile with Auger electron spectroscopy (see Fig. 3).

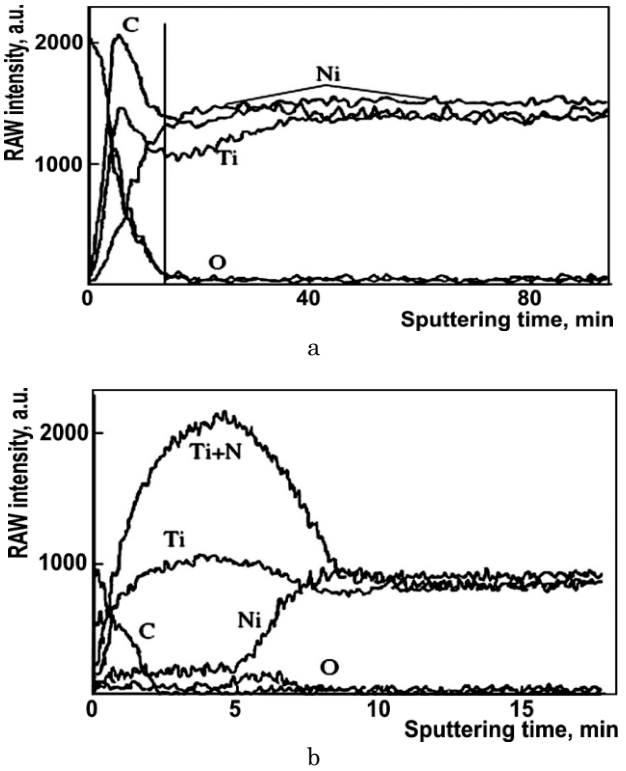

Fig. 3 – Auger electron spectroscopy data for unimplanted NiTi samples (a) and NiTi samples implanted at an energy of 65 keV and a dose of 5×10^{17} ion/cm^2 (b)

a

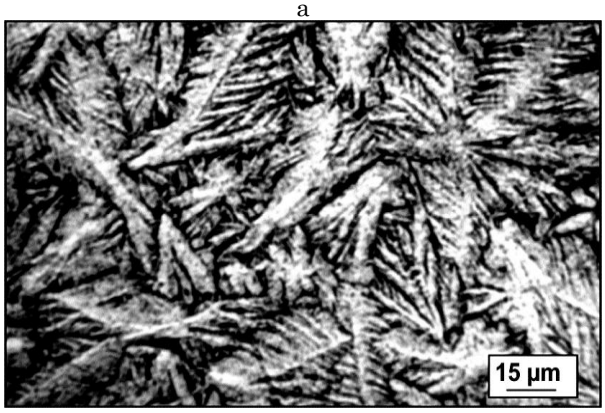

b

Fig. 4 – Optical micrographs of the cross-section of a NiTi alloy with a martensitic structure and SME before implantation. (b) Optical micrographs after ion implantation

This profile indicates that the penetration depth of N^+ ions is about 280-200 nm. After sputtering for 10 min the concentrations of nickel and titanium ions are seen to level off and reach their intrinsic levels (49.9 and 50.1 at. % Ni and Ti in the crystal lattice of the NiTi alloy, respectively).

Fig. 4 shows optical microscopy data. They demonstrate a typical martensitic structure and changes in the martensitic structure after implantation.

The surface layer of the implanted sample has a significant concentration of nitrogen and oxygen and the characteristic eating away is observed in the spectrum of NiTi implanted sequentially by nitrogen and nickel. We used a standard computer program and determined the nitrogen concentration from the eating away in the spectrum and plotted element-concentration profiles. The eating away appears when a light element is added to a heavy-element matrix.

Fig. 5a shows the spectrum of helium ions sputtered by the implanted sample. Among the light elements, only oxygen exhibits a peak; however, oxygen is located near the sample surface and the eating away is caused by nitrogen. Fig. 5b shows the spectrum of protons scattered by the initial implanted sample. Although titanium is seen to be distinguished from nickel and iron, light impurities are not detected. The surface layer of the implanted sample has a significant concentration of nitrogen and oxygen and the characteristic eating away is observed in the spectrum of NiTi implanted sequentially by nitrogen and nickel.

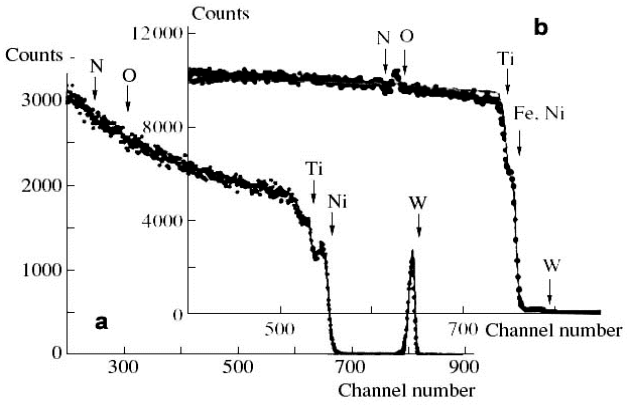

Fig. 5 – Rutherford backscattering spectrum (2.035 MeV helium ions) of a NiTi sample after 60 keV N ion implantation at a dose of 10^{18} cm^{-2} followed by implantation of Ni ions at a dose of 5×10^{17} cm^{-2} and a voltage of 60 kV (a). The spectrum recorded on the same sample with protons at an energy of $E = 2.012$ MeV (b)

When analyzing the profile of N^+ ions in NiTi (Fig. 6), we see that the nitrogen profile has a double-humped shape: one con-centration maximum is located near the surface (the maximum concentration is about 36 at. %). and the second peak is located at a depth of more than 130-150 nm (133 at Å2 and has a lower concentration (27 at. %). In the valley between the two nitrogen concentration maxima, the concentration of Ni+ ions is maximal (about 20 at. %). Since the titanium or nickel concentration in the initial state is about 50 at. %, this point was taken as an initial. We can find out the error in determining the concentration of nitrogen ions – it equals 5 at. %. The error in determining the nickel concentration for concentration profiles was 1.2 at. %. The nickel profile was plotted beginning from 50 at. %.

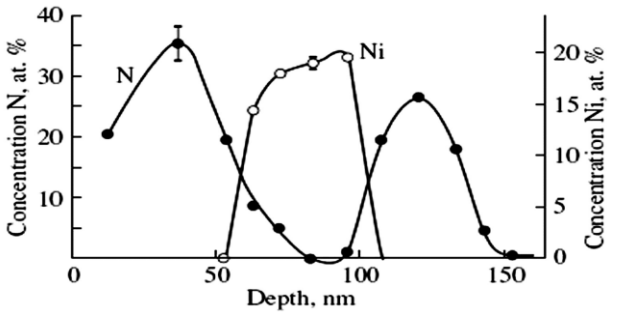

Fig. 6 – Depth profiles of the element concentrations obtained from energy spectra of the NiTi sample surface after double implantation of N ions at a dose of 10^{18} cm^{-2} and Ni ions at a dose of 5×10^{17} cm^{-2}

Moreover, preliminary SIMS (secondary-ion mass spectrometry) studies also demonstrate the formation of a double-humped nitrogen concentration profile. However, the nitrogen concentrations in the maxima slightly differ from the RBS data, which is caused by the higher threshold of delegability of SIMS ($\sim 10^{-5}$ at. %).

Three NiTi phases are important in shape memory phenomena. High temperature phase (austenite) has an ordered CsCl or B_2-type lattice. So-called "R-phase"

with rhombohedral crystal lattice may form first upon cooling at T_R temperature. The second type of martensite has the monoclinic $B_{19'}$ lattice. Transformation temperatures depend on chemical composition and structure of the NiTi alloy.

The R-phase is commensurate with B_2 lattice. Instability of B_2 structure and formation of so called incommensurate phase always precedes the formation of R-phase. The two sequences of phase transformations are possible in binary NiTi alloys [2, 20, 21]:

I $B_2 \rightarrow$ incommensurate phase $\rightarrow$ R $\rightarrow B_{19'}$, or
II $B_2 \rightarrow B_{19'}$.

The R-phase formation precedes the $B_{19'}$ transformation when the Ms temperature is lowered ($M_S < T_R$). Increase of Ni content with respect to Ti, work hardening, and aging can depress the M_S and yield the R-phase formation [20-22]. The R-phase transition is typified by extremely narrow thermal hysteresis (1 to 2 °C). whereby thermal hysteresis related to $B_{19'}$ may vary from approximately 20 °C to hundreds of degrees [21]. The effective control of transformation temperatures can be accomplished by alloying the binary NiTi system with other elements. Formation of orthorhombic martensite B_{19} instead of R-phase and $B_{19'} \rightarrow$ triclinic $B_{19''}$martensite transformation has been detected in ternary systems.

The factors that influence the deformation behavior, corrosion behavior and shape memory parameters of NiTi alloys [2, 21, 22] are:

1. chemical composition (content of Ti, Ni, alloying elements and impurities);
2. dislocation density and grain size of austenitic phase;
3. presence of coherent precipitate.

Any operation related to change of dislocation density and grain size, diffusion, and precipitation processes changes the transformation temperatures of NiTi. This is extremely important because the high temperature shape to be "memorized" by a NiTi alloy is most typically imparted at temperatures between 400 to 600 °C. Varying chemical composition, thermal and mechanical treatment of NiTi alloys represent an important tool in tailoring their performance. Recoverable strains during SME and PE in NiTi polycrystals vary up to 8 % and generated stresses up to 1000 MPa have been reported. Increasing of dislocation density after cold working leads to decreasing in recovery strain because of interface movement limitations (pinning). Work-hardened materials yield higher generated stresses compared to annealed NiTi alloys [2, 23, 24]. The M_S temperature decreases and the T_R and As temperatures increase after work hardening. Introduced structure defects result in widening of thermal hysteresis and widening of intervals between Ms and M_f or As and A_f respectively. The orientation dependence of properties, especially in the case of wrought NiTi specimens, is typically observed [2, 20, 23]. The structure parameters will also determine fatigue lifetimes.

In the process of nitrogen ion implantation with the fluence 10^{18} cm^{-2} and 50 keV of energy, the well-defined double-layer structure with different microstructure as well as different phase and chemical composition was formed (Fig. 7). During ion implantation, collisions between the incident ions and the NiTi-target atoms lead to the formation of near-surface amorphized layer *(*A-layer) and the extended defects in the crystalline structure of bulk material *(*D-layer, Bulk).

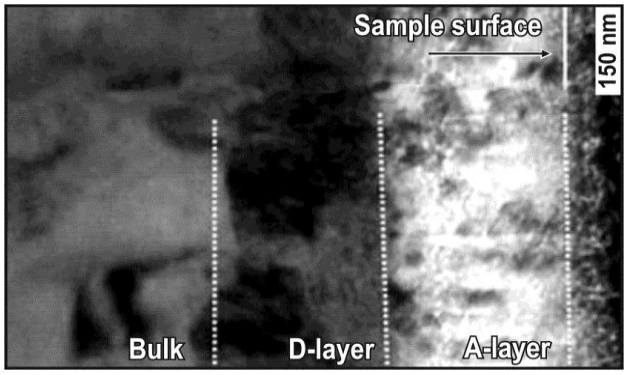

Fig. 7 – Bright-field image of the ion-implanted NiTi alloy demonstrating the structure near-surface layers

The transition zone of a damaged region is wide and its composition changes gradually from totally amorphized Ti-rich material (heavily damaged and nanocrystalline) to Ni-rich crystalline (A-layer in Fig. 7). Amorphous-like layer contains some amount of crystalline inclusions within its bulk, mainly near a bottom boundary of the transition zone. This confirms the fact that the amorphization process occurs faster from the depth of maximum damage regions towards the sample surface than in its bulk.

The NiTi samples implanted by N^+ ions are seen to have a higher (by 15-20 %) hardness than the initial samples. The changes in the SME (Fig. 8) demonstrate that the implanted NiTi alloy exhibits an indentation with a higher hardness after recovery as a result of healing to 75 °C. In other words, all mechanical changes related to the SME and mechanical properties (hardness) are interrelated with the elemental composition and micro-structure of the material.

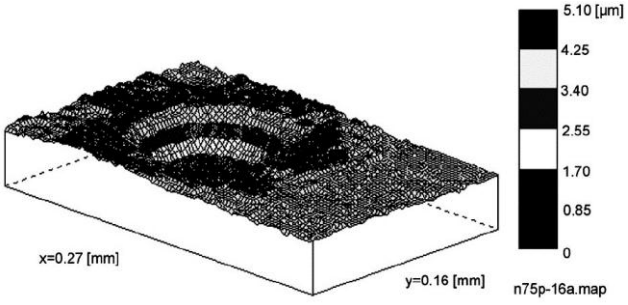

Fig. 8 – SME measurements (with a scanning profilometer) on a TiNi sample after heating to 75 °C

Fig. 9 shows the results of loading and unloading (at loads of 4 and 7 *N*) the samples before and after implantation at doses of 5×10^{17}-10^{18} cm^{-2}.

The hardness H and the elastic modulus E were determined using a nanohardness measuring device (Nanoindenter II) according to the Oliver-Pharr and Berkovich indentation methods. The hardness H and Young's modulus E data change correspondingly. Their values were determined at various depths (see Table 1).

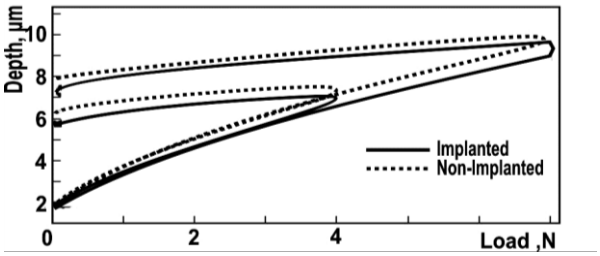

Fig. 9 – Indentation curves for implanted and unimplanted TiNi samples exhibiting SME recorded at various loads

Table 1 – Hardness and elastic modulus of TiNi samples

	Sample	*E*, GPa	*H*, GPa
	depth of 150 nm		
1	Initial	56 ± 2	2.13 + 0.30
2	W + Mo	59 + 11	2.78 + 0.95
3	W + Mo after annealing	298 + 81	4.11 ± 0.35
	depth of 50 nm		
4	Initial	56 ± 4	2.74 + 0.30
5	W + Mo	59 + 8	4.95 + 2.26
6	W + Mo after annealing	236 + 39	4.44 ± 1.45

The hardness is seen to increase from 2.13 ± 0.13 to 2.78 ± 0.95 GPa at a depth of 150 nm. The elastic modulus varies from $E = 56 \pm 2$ to 59 ± 11 GPa. After annealing at 550 °C for 2 h, these values increase sharply: $H = 4.11 \pm 0.35$ GPa, $E = 289 \pm 81$ GPa. Small differences between the hardness and elastic module of the initial, implanted and annealed samples are also detected at a depth of 50 nm. Upon implantation, we have $H = 4.96 \pm 2.26$ and $E = 59 \pm 8$ GPa; after annealing, we have $H = 4.44 \pm 1.45$ and $E = 236 \pm 39$ GPa (the elastic modulus increases by a factor of almost 4.5).

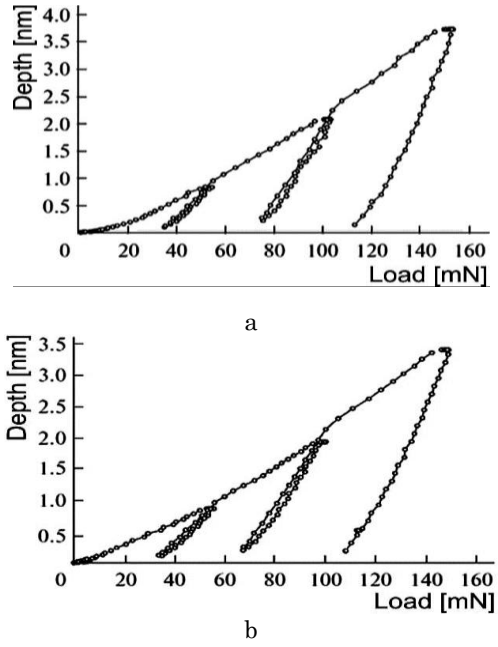

Fig. 10 – A diagram of indentation penetration for an initial sample (a) and after implantation (b)

A value of elastic recovery W_e of a surface layer was calculated using the curves "loading-unloading". The penetration diagrams are shown in Fig. 10 a, b.

A peculiarity of given diagrams is essentially high for a metal elastic recovery in indentor unloading. This indicates a low modulus of E elasticity with a relatively high hardness H (a value of the elastic recovery was determined by the ratio E/H). A desired load for indentor penetration to 50 nm depth was minimum for the initial sample (0.8-0.1 mH), it was increased to (0.9-0.1 mH) for an implanted sample and it was maximum for an implanted sample after annealing (1.2-0.1 mH). This indicates growing hardness of the surface layer after implantation and annealing. The fact that an elastic recovery of a print depth in unloading after annealing was much longer than that for an initial one is worth our attention. This indicates that hardness growth was accompanied by weak modulus enhancement, i.e. hardness after implantation and annealing increased more significantly than the elastic modulus.

Investigation of the influence of nitrogen ion implantation on the wear resistance of shape memory material was carried out on samples from equal to the atomicalloy NiTi (Nitinol, Shape Memory Corporation, Japan) in the martensitic phase. Samples of size 22 × 5,4 × 0,3 mm annealed for 30 min in a vacuum oven at 583 K, and then washed in a solution of 10 % $NClO_4$ 90 % CH_3COOH. Nitrogen implantation was carried out at doses of $D_1 = 1 \times 10^{17}$ cm^{-2}) and $D_2 = 2 \times 10^{18}$ cm^{-2}) at a beam energy of 50-65 keV ions. The wear resistance of the surface layer at friction was carried out using a sapphire ball tribological tester 6 mm in diameter with a piston sliding without lubrication on the surface of the material.

In testing, the ball was loaded with a load of 0.4 N and 0.70 N, and the amplitude of the reciprocating motion of the ball was 3 mm. The wear resistance of non-implanted and implanted (doses D_1 and D_2) samples of alloy NiTi was investigated. The time of the test was 1, 3, 6 and 12 hours. In order to obtain reproducible results for each attempt (for different values of load and time) tests for all samples were repeated three to five times. Signs of wear (tracks) in the form of grooves were visible on the surface of the load after moving the ball. The wear degree of material can be inferred by the depth of the furrows.

Measure of ash material can serve as the volume of the furrow. Additionally, the wear test was carried out in profilometrics measurements obtained by furrows, which allowed the comparison of surface morphology. Using the software, Hommel Map Expert maps were constructed surface under study that allow to show signs of wear on the surface of NiTi.

Modified samples showed greater resistance to abrasion of the surface layer compared to non-implanted material after ion implantation. The dependence of the material NiTi flow before and after ion implantation during "dry sliding" friction in the test of time (under a load of 0.7 N and 0.4 N) is shown in Fig. 11. For both loads (0.4 N and 0.70 N) at any time in the abrasion test the amount of material blown from the implanted samples was lower than for non-implanted material. In the case of load 0.4 N (Fig. 11a) at a dose of implantation D_2 increased wear resistance was higher not only compared to non-implanted samples, but also in comparison with the samples modified at a lower dose of D_1.

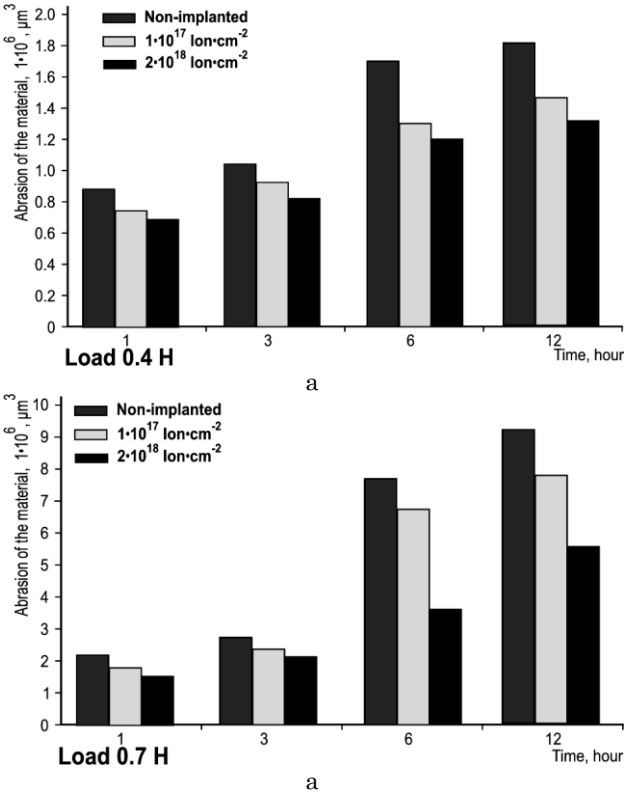

Fig. 11 – Consumption NiTi before and after ion implantation ($D_1 = 1 \times 10^{17}$ cm^{-2} and $D_2 = 2 \times 10^{18}$ cm^{-2}) during "dry sliding" test of time: for the load 0.4 *N* (a) and consumption NiTi for the load 0.7 *N* (b)

The difference between the ash materials is negligible for all samples after 1 h of friction ball. Significant differences in the amount of material blown from the non-implanted and implanted samples are visible during the test due to friction at 3h, 6h and 12h. As can be seen from Fig. 11b, at a load of 0.7 *N* the wear resistance of samples implanted with a dose of D_2 NiTi increases not only in relation to the non-implanted samples, but also in relation to lower dose implanted samples.

The surface NiTi sample after double implantation by N^+ and Ni^+ ions is rather rough ($\alpha = 0.8$-1.2 μm) due to sputtering mainly by nitrogen atoms. This surface was subjected to electron-probe microanalysis. The following elements were detected in the near-surface layer: N (~ 2.1 at. %), O (~ 5.61 at. %, C (~ 0.58 at. %), Ni (~ 49.43 at. %), and Ti (~ 41 at. %). To detect Ti, we used another detector.

The low (as compared to the RBS data) titanium concentration is caused by the larger depth of SEM as compared to EDS (which is 2.2 μm). Moreover, the nitrogen ion range is almost 300 nm at the energies (60-70 keV) used in our experiments. Upon implantation, the elastic modulus increases insignificantly; however, after heat treatment, it increases to 236 ± 39 or 289 ± 80 GPa (i.e., by a factor of 4-4.5 compared to the initial state).

The coating demonstrated the increased corrosion resistance in acidic and alkaline media in comparison with that of the non-implanted surface.

4. CONCLUSIONS

The development of NiTi based SMA thin films and their microactuators has achieved considerable progress in recent years. This was largely driven by a fast expansion of, in particular, microelectromechanical system and biological communities, in which the demand for novel actuators and biological applications have been growing dramatically. As such, a timely review of the important issues pertaining to the preparation of high quality and high performance shape memory NiTi thin films and the technical applications of these films are necessary.

It is shown that the sequential double implantation of N^+ and Ni^+ ions into nitinol (NiTi) leads to the formation of a complex depth profile of the nitrogen concentration, which is caused by the rejection of nitrogen ions from the region of the maximum Ni^+ ion losses (i.e., the region of the maximum Ni^+ ion concentration) to the region of residual tensile stresses. As a result of the implantation of N^+, Ni^+, W^+, and Mo^+ ions, the hardness after implantation increases by 30 % compared to the initial state and the hardness after subsequent thermal annealing at 550 °C for 2 h increases by a factor of 2.2. The SME changes because of the formation of nitrogen and carbon (carbonitride) layers as a result of N^+ implantation and because of a change in the concentrations of Ti and Ni atoms due to the sputtering of Ni atoms, which is accompanied by a change in the martensite transformation temperature.

The martensitic form of equiatomic NiTi was implanted with N ions with the fluence 10^{18} cm^{-2} and 50 keV energy. To characterize the transformation sequence and transformation temperatures, the DSC measurements were carried out on a non-implanted as well as an implanted material. Both the non-implanted and ion-implanted NiTi alloys transform in two steps ($B_2 \rightarrow R \rightarrow B_{19}$) in the cooling direction and one-step transition ($B_{19} \rightarrow B_2$) in the heating process. The X-ray structural investigations were performed to verify identifications of martensitic transformations in the NiTi alloys during heating and cooling. The TEM structural characterization reveals the existence of the well-defined double-layer structure with different microstructure as well as different phase and chemical composition in the near-surface region of the ion-implanted Ni'Ti alloy. The sample has an amorphized structure in the form of two sub-layers: the first is a Ti- and N-rich nano-crystalline and/or amorphous-like and the second is Ni-rich crystalline from the surface to a depth of 80 nm. In the depth of 80-160 nm the material has a defected Ti-rich crystalline microstructure and deeper - an unaffected grain structure of the parent material.

Some important issues pertaining to the preparation of high performance shape memory NiTi films using sputtering methods and their applications were reviewed in this paper. Successful application of NiTi thin films requires consideration of the following issues: preparation and characterization, residual stress and adhesion, frequency improvement, fatigue and stability, patterning and modeling of behavior. NiTi film based micoractuators will find potential applications in medicine, aerospace, automotive, and consumer products. Miniature NiTi actuated devices based on sputtered NiTi films are ready for the huge commercial market, especially for medical microdevices and implantable applications.

Высокодозная ионная имплантация в NiTi для улучшения эффекта памяти формы и псевдопластичности

А.Д. Погребняк[1], С.Н. Братушка[1], Н. Левинтант-Заяц[2]

[1] *Сумский государственный университет, ул. Римского-Корсакова, 2, 40007 Сумы, Украина*
[2] *Институт фундаментальных исследований ПАН, Варшава, Польша*

В статье представлены новые результаты исследования влияния высокодозной ионной имплантации ионов N, Mo, W, N и Ni дозой 10^{18} см$^{-2}$ на физико-механические свойства сплава: увеличение износостойкости сплава при истирании поверхностного слоя, увеличение нанотвердости, устойчивости к коррозии, а также изменения морфологии поверхности NiTi. Обнаружено корреляцию между изменением элементного состава поверхности после имплантации и изменением механических свойств сплава. Иными словами, в результате высокодозной ионной имплантации в поверхностном слое формируется наноструктура оксикарбидов и оксинитридов, которая повышает износостойкость, коррозионную стойкость и нанотвердость материала. В то же время, объемные свойства NiTi (псевдопластичность и эффект памяти формы) после имплантации не меняются, что позволяет применять ионную имплантацию в качестве эффективного инструмента для улучшения свойств материалов.

Ключевые слова: Имплантация, NiTi, Эффект памяти формы, Псевдопластичность, Свойства.

Високодозова іонна імплантація в NiTi для поліпшення ефекту пам'яті форми та псевдопластичності

О.Д. Погребняк[1], С.М. Братушка[1], Н. Левінтант-Заєць[2]

[1] *Сумський державний університет, вул. Римського-Корсакова, 2, 40007 Суми, Україна*
[2] *Інститут фундаментальних досліджень ПАН, Варшава, Польща*

У статті представлені нові результати дослідження впливу високодозової іонної імплантації іонів N+, Mo, W, N та Ni дозою 10^{18} см$^{-2}$ на фізико-механічні властивості сплаву: збільшення зносостійкості сплаву при стиранні поверхневого шару, збільшення нанотвердості, стійкості до корозії, а також зміни морфології поверхні NiTi. Виявлено кореляцію між зміною елементного складу поверхні після імплантації і зміною механічних властивостей сплаву. Іншими словами, в результаті високодозової іонної імплантації в поверхневому шарі формується наноструктура оксикарбідів та оксинітриду, яка підвищує зносостійкість, корозійну стійкість і нанотвердість матеріалу. У той же час, об'ємні властивості NiTi (псевдопластічність і ефект пам'яті форми) після імплантації не змінюються, що дозволяє використовувати іонну імплантацію як ефективний інструмент для поліпшення властивостей матеріалів.

Ключові слова: Імплантація, NiTi, Эфект пам'яті форми, Псевдопластичність, Властивості.

REFERENCES

1. *Ion Implantation* (Ed. by J.K. Hirvonen) (London: Academic Press, Inc.: 1980).
2. A.D. Pogrebnjak, A.P. Kobzev, B.P. Gritsenko, S. Sokolov, E. Bazyl, N.V. Sviridenko, A.N. Valyaev, Yu.F. Ivanov. *J. Appl. Phys.* **87**, 2142 (2000).
3. O.M. Ivasishin, A.D. Pogrebnjak, S.N. Bratushka, *Nanostructured layers and coating formed by ion-plasma fluxes in titanium alloys and steels* (Kyiv: Akademperiodyka: 2011).
4. L.L. Meisner, A.I. Lotkov, M.G. Dementyeva, N.N. Koval, Yu.F. Ivanov, E.Yu. Gudimova, *Rare Metals* **28**, Spec. Issue October, 361 (2009).
5. A.M.C. Pérez-Martin, A.M. Vredenberg, L. De Wit, J.S. Custer, *Mater. Sci. Eng. B* **19**, 281 (1993).
6. D. Chrobak, H. Morawiec, *Scripta Mater.* **44**, 725 (2001).
7. S. Shabalovskaya, J. Andregg, J. Van Humbeeck, *Acta Biomater.* **4**, 447 (2008).
8. S.-Y. Сна, J.S.-Y. Jeonc, J.H. Park, S.E. Park, J.K. Park, C.R. Cho, *J. Korean Phys. Soc.* **49**, 580 (2006).
9. K.K. Kadyrzhanov, F.F. Komarov, A.D. Pogrebnjak, V.S. Rusakov, T.E. Turkebaev, *Ion-Beam and Ion-Plasma Treatment of Materials* (Moscow: Moscow State Univ.: 2005).
10. A.D. Pogrebnjak, S.N. Bratushka, V.V. Uglov, V.S. Rusakov, V.M. Beresnev, V.M. Anischik, L.V. Malikov, N. Levintant, P. Zukovski, *Vacuum* **83**, 6, S240 (2009).
11. D.M. Shirokov, V. Bohac, *NIMPR B* **84**, 497 (1994).
12. T. Czeppe, N. Levintant-Zayonts, Z. Swiatek, M. Michalec, O. Bonchyk, G. Savitskij, *Vacuum* **83**, S214 (2009).
13. A.D. Pogrebnyak, S.N. Bratushka, N. Levintant, N.K. Erdybaeva, S.V. Plotnikov,B.P. Gritsenko, *Tech. Phys.* **54** No5, 667 (2009).
14. V.I. Lavrentiev, A.D. Pogrebnjak, *Surf. Coat. Tech.* **99**, 24 (1999).
15. A.D. Pogrebnjak, E.A. Bazyl, *Vacuum* **64**, 1 (2001).
16. A.D. Pogrebnjak, O.G. Bakharev, N.A. Pogrebnjak, Yu.V. Tsvintarnaya, V.T. Shablja, R. Sandrik, A. Zecca, *Phys. Lett. A* **265**, 225 (2000).
17. A.D. Pogrebnjak, A.P. Kobzev, B.P. Gritsenko, S. Sokolov, E. Bazyl, N.V. Sviridenko, A. Valyaev, S.V. Plotnikov, *Jpn. J. Appl. Phys.* **38**, L248 (1999).